Received: 16 April 2021 | Revised: 20 August 2021 | Accepted: 21 August 2021

DOI: 10.1002/er.7237

RESEARCH ARTICLE

INTERNATIONAL JOURNAL OF ENERGY RESEARCH WILEY

Performance improvements in Stirling cycle machines by a modified appendix gap geometry

Jan Sauer | **Hans-Detlev Kühl**

Lehrstuhl für Thermodynamik (BCI), TU Dortmund University, Dortmund, Germany

Correspondence
Hans-Detlev Kühl, Lehrstuhl für Thermodynamik (BCI), TU Dortmund University, Emil-Figge-Straße 70, 44227 Dortmund, Germany
Email: hans-detlev.kuehl@tu-dortmund.de

Funding information
German Research Foundation (DFG), Grant/Award Number: KU 755/4-1 & 2; Technische Universität Dortmund

[Correction added on 14 December 2021, after first online publication: Equations 15, 17, and A10 have been corrected.]

Summary

In this contribution, the optimization potential of the seal geometry in Stirling machines is explored both numerically and analytically, leading to a significant reduction of the related losses which are often referred to as appendix gap losses. These are induced by the narrow gap between the displacer and the cylinder and have mostly been underestimated so far. A recent experimental investigation revealed large optimization potentials by reduction of the seal and cylinder wall diameter near the seal, resulting in reduced appendix gap losses and further indirect positive effects. In this work, these experimental findings could be reproduced by a one-dimensional differential simulation model at a fully satisfyingaccuracy. Furthermore, these investigations reveal that the optimum geometry is largely machine-dependent. To provide an easily applicable design rule for this optimum geometry, a refined analytical model for the mass flow at the top of the gap is derived, which is based on a phasor analysis and a linearized mass balance that also accounts for changes in the spatial mean gas temperature in the gap. The optimum design predicted by this model is very close to numerical optimization results and sufficiently accurate under practical aspects. Furthermore, this model contributes to a better theoretical understanding of the loss mechanisms in the gap.

KEYWORDS

analytical calculation, numerical simulation, optimization, Stirling cycle

1 | INTRODUCTION

Regenerative cycles, such as the well-known Stirling cycle, may utilize and transform virtually any heat flow, particularly including heat from various renewable sources, and may thus contribute to the global energy transformation. Therefore, they are increasingly under consideration for micro-cogeneration applications[1-4] and particularly for utilizing various forms of biomass[5-11] as well as solar energy.[12-15] However, the performance of the idealized, theoretically reversible cycles is in practice degraded by a variety of loss mechanisms. Therefore, the design of a sufficiently efficient machine is a complex optimization problem requiring accurate models for these. One of these losses is the appendix gap loss. It is caused inside the gap around the insulating, thin-walled piston or displacer, as this gap is open to a cylinder volume at either hot or cryogenic temperature level. In kinematic Stirling engines or coolers, this gap is typically closed by a sliding seal at the end where the near-

ambient temperature prevails. Particularly in the so-called β- and γ-types featuring a double-acting displacer, gas leakage across the seal is usually negligible since the pressure difference is only induced by flow pressure losses and therefore marginal. In free-piston Stirling machines, the gap instead features a close-tolerance seal only or is even intentionally left open to serve as a regenerative annulus.[16,17] However, this case will be excluded here. Instead, the following considerations refer to a closed gap in a kinematic machine, ignoring any seal leakage. In this case, the appendix gap loss is usually considered to be a superposition of two different mechanisms, which are commonly referred to as the shuttle loss and the enthalpy loss.[18-25] The former was qualitatively known from cryocoolers as "motional heat transfer" before[26] and later also referred to as "bucket brigade loss,"[27] the latter is also known as "pumping loss."[28]

In general, any accurate modelling of regenerative cycles requires consideration of the various loss mechanisms including their multiple interactions, which is only possible by a differential approach. In recent years, even two- and three-dimensional CFD models of whole engines have therefore been developed.[29-35] However, the computational expense for a multi-parameter optimization on this basis is considerable. So, there are still good reasons to apply spatially one-dimensional differential models (the so-called "third-order models"), which may also account for interdependencies between the loss mechanisms, but require far less computing time. Such models have been developed repeatedly since the 1970s, applying various discretization and integration techniques and more or less rigorous handling of the momentum equation in particular. Remarkably, the comparatively recent and very rigorous model by Andersen[36] was the very first to include the appendix gap in the differential simulation, whereas in the earlier models, the associated loss was either neglected or estimated separately based on simplified analytical models and finally superimposed upon the differential simulation results - presumably because it was generally considered to be of minor importance only.

However, Andersen et al[37] observed that according to their differential simulation, this loss was higher than anticipated. Experimental results performed by Geue et al[38] using a well-instrumented convertible, experimental machine[38-41] qualitatively supported this finding. So, a critical review of the available analytical models was performed by Pfeiffer and Kühl[42] and subsequently, a refined analytical model which accounts for the unsteady, oscillatory laminar flow in the gap was developed and applied to further optimize the gap geometry and particularly the seal design.[43-45] It should be mentioned here, that in this analytical model as well as in the numerical models discussed, temporally constant wall temperature profiles are implicitly assumed. This is essentially correct in the case of metallic wall materials, which are typically found in Stirling engines as well as in the aforementioned machine since in this case, the amplitude of the wall surface temperature oscillations is in the range of a few tenths of a Kelvin only. Any effects caused by low-conductivity coatings[46,47] or by the use of polymer materials in cryogenic applications[23,48] are therefore neglected within this contribution.

Recently, the unsteady gas temperature profiles predicted by this model have essentially been confirmed experimentally by Sauer and Kühl,[49] once again using the aforementioned experimental machine.[50] Since the design of this machine is the result of a similarity-based scaling procedure[39] and therefore features an extremely large gap width of $h = 1.4$ mm, this was possible by inserting radially adjustable fine wire thermocouple probes in the gap and thus directly measuring the fluctuating gas temperatures at a high spatial and temporal resolution.

According to the analytical model, which can be considered experimentally validated by these investigations, the appendix gap loss is actually higher than predicted by the previously available models, particularly if the gap width h is optimized according to the latter. The new model generally yields a smaller optimum gap width than these, and furthermore, it indicates that the loss may be substantially reduced by a reduction of the effective seal diameter below the diameter of the cylinder wall in the range of the open gap above, almost down to the lower limit imposed by the diameter of the displacer (or piston, respectively). This design modification results in a reduced gap width h_0 in the bottom section of the gap designating the remaining clearance between the liner and the displacer in the vicinity of the seal, as illustrated in Figure 1. It may be specified by the dimensionless ratio

$$r_h = \frac{h_0}{h}, \tag{1}$$

which will be referred to as the gap width ratio in the following.

In a recent experimental investigation reported by Sauer and Kühl,[49] such a modification was realized in the experimental machine by mounting a seal with an outer diameter marginally above that of the displacer and by inserting a cylinder liner with an accordingly reduced inner diameter. Due to constructional limitations, a minimum bottom gap width $h_0 = 0.3$ mm could thus be realized, which will be referred to as "new" seal design in distinction to the "old" seal design. This corresponds to a

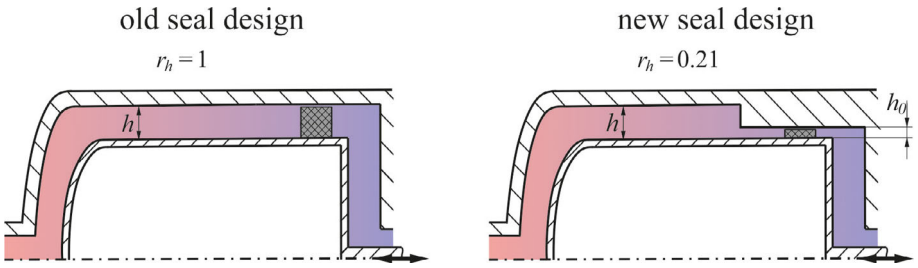

FIGURE 1 Schematic illustration of the old and the new seal design

value $r_h = 0.21$, which is very close to the analytically predicted optima in Vuilleumier mode and Stirling mode, which are $r_h = 0.2$ and $r_h = 0.1$. The new and old seal design is shown in Figure 1.

The effects of this modification were carefully studied using the available instrumentation and compared to the previously obtained experimental results.[49] Thus, a decrease of the appendix gap loss could be confirmed, and furthermore, it was found that there was virtually no reduction of the pressure amplitude, which had initially been expected due to the reduced volumetric displacement. Both the mechanical net power in Stirling mode and the refrigeration capacity in Vuilleumier mode of the convertible experimental machine consequently remained constant or were even slightly increased, whereas the hot end heat input was noticeably reduced. So, the observed improvements of the overall cycle performance substantially exceeded the initial expectations, which were based on the loss reduction as predicted by the analytical model. According to Sauer and Kühl,[49] these can presumably be attributed to the following effects:

- A detailed analysis of the thermal compression effects caused by the moving displacer reveals that the actual temperature change of the gas quantity additionally displaced at large values of r_h is marginal because this quantity - or rather two corresponding quantities of the same size - are either located below the seal, i. e. in the cylinder volume maintained at the lower, "cold" temperature T_c, or directly above the seal, i. e. in the bottom section of the gap, where a similar temperature is imposed by the adjacent cylinder wall.
- In the case of $r_h \to 1$, the additionally displaced gas quantity causes an additional flow through the heat exchangers and the regenerator as well as along the length of the gap, which can be avoided for $r_h \to 0$. The corresponding reduction of the pressure drop by flow losses could be experimentally confirmed.
- In addition to this, the reduced gas flow through the regenerator in the case of $r_h \to 0$ will also result in correspondingly smaller thermal regenerator losses, contributing to a further reduction of the net heat exchange via the heater and the cooler in addition to the lower appendix gap loss and the smaller pV works of the corresponding cylinder volumes.
- The lower loads at the heat transfer result in a corresponding decrease of the required temperature differences for the heat transfer and thus in an enhancement of the thermal compression.
- The dead volume of the gap is decreased in the case of $r_h \to 0$, which helps to maintain the pressure amplitude.

These indirect effects can of course not be predicted by any separate analytical model for the appendix gap loss, and so, there is an obvious need to directly include the gap in a differential simulation of the entire cycle, as first realized by Andersen.[36]

It is the objective of this contribution to reproduce the aforementioned experimental findings by such a model, to perform further optimizations on this basis beyond the limitations of the available experimental facilities, to improve the theoretical understanding of the underlying mechanisms by means such as phasor analysis, and to finally derive an analytical tool to predict the optimum gap geometry, particularly regarding the seal diameter.

However, this simulation model is not publicly available, and furthermore, it requires considerable computation times due to the rigorous handling of the momentum equation. Consequently, it was decided to extend the modularly structured, one-dimensional simulation code *kpsim* developed at TU Dortmund University by a component of the cylinder comprising a differentially modelled gap.[51] This code is based on a simplified handling of the momentum equation and a comparatively coarse spatial resolution of the pressure field, which is assumed to be close to equilibrium. Thus, it is possible to integrate the resulting equation system at comparatively large time step widths, and in combination with an efficient convergence acceleration technique, computing times of a few seconds only on a modern personal computer can be realized.

The differential model for the gap was realized in a similar way as reported by Andersen et al,[37] i. e. by discretizing the gas volume in the gap as well as the cylinder

and the displacer wall by an adjustable number of finite volume elements. However, when performing simulations including the differential model for the gap, a problem already reported by Andersen et al was encountered, namely that the results were found to be severely dependent on the chosen modelling approach for the radial heat exchange between the gas and the walls.

Basically, any spatially one-dimensional differential approach requires separate modelling of any transport phenomena perpendicular to the discretization direction. Whereas a variety of experimentally validated approaches exist for the flow conditions in typical heat exchangers and regenerators, Andersen et al[37] as well as Sauer and Kühl[51] only had a choice between a few empirical approaches lacking a sufficient experimental and theoretical basis. In common one-dimensional differential models, the assumption of an ideal plug flow is implicitly made. However, the question arises whether this assumption is justified in the description of the axial energy transport by the unsteady, laminar gas flow in the gap featuring a both temporally and radially variable temperature profile according to the analytical model by Pfeiffer and Kühl.[43] To resolve these issues, Sauer and Kühl[52] derived a new approach for the radial heat exchange between the gas and the walls as well as for the energy transport by the axial gas flow based on the aforementioned analytical model and the supporting experimental findings.[50] Due to its theoretical and experimental basis, this approach was subsequently used as a reference model for comparison purposes, and it was found that in the exemplary cases investigated so far, a less complex, semi-empirical approach by Andersen et al,[37] which is based on the assumption of parabolic temperature profiles in the radial direction and a plain plug flow assumption, is sufficiently accurate. As a result, a tool is available now that allows more detailed numerical investigations in the gap section. It yields a good agreement between experimental and simulated data for the experimental machine on the basis of a revised and validated input data set.[52]

2 | NUMERICAL SIMULATION AND OPTIMIZATION

For the simulation of different seal geometries, such as a decreased diameter of the cylinder liner in the range of the seal, the cylinder component described in Reference 51 was modified marginally. The size of the cylinder volume, which so far underwent all volumetric changes of the cylinder component, is further on evaluated with the cylinder diameter at the top. Therefore, the finite gas volumes in the gap, which were constant and equal in size so far, may now undergo volumetric changes as well. If a finite volume reaches the edge of the liner, where the gap width is reduced from h to h_0, its size changes, and consequently, the p,V-work done by this volume change is considered in the energy balance. The discretization of the cylinder system including the gap is illustrated in Figure 2, where $\hat{x}$ and l_a denote the stroke amplitude and the appendix gap length.

2.1 | Comparison of experimental and simulated results

The simulation accuracy of the program *kpsim* has been demonstrated repeatedly, inter alia for the considered experimental machine.[38,40,52] However, the modification of the simulation code must also be validated. The generally most sensitive criterion for this purpose is the reproduction accuracy of experimental p,V-plots. Figure 3 shows a comparison for the p,V-loops in Stirling mode for both seal designs at the nominal conditions summarized in Table 1, which also applies to Vuilleumier mode operation. Further details concerning the design of the experimental machine and the toggling between these modes are reported in Reference 49.

Evidently, the simulation accuracy is good in either case, and in particular, it is unaffected by the modification, which is barely visible at first sight but can be detected as a small change in the amplitudes of the hot and the warm cylinder volume. However, it is not the purpose of these plots to visualize the modification of the effective seal diameter, but to prove that the simulation code is able to reproduce the experimental performance satisfactorily in either case, i. e. that the modification of the code described in the previous chapter does not affect its accuracy. In the Vuilleumier mode, the simulation accuracy is even better in general. Based on this, the corresponding heat flows can be reliably compared, which is shown in Figure 4 for both seal designs in Vuilleumier mode. The experimental data correspond to the data shown in Reference 49, but without error bars for reasons of clarity. Additionally, Figure 4 presents the sum of simulated appendix gap losses and axial heat conduction along the walls.

Apparently, the simulation reveals a strong decrease of the heat input for the new design that even exceeds the reduction of the losses directly associated with the gap and the surrounding walls, although it is smaller than the experimentally observed decrease and at generally lower values. In contrast to the experimental results, the simulation furthermore indicates a small decrease in the refrigeration power. However, this decrease is in the range of the measurement uncertainty for the

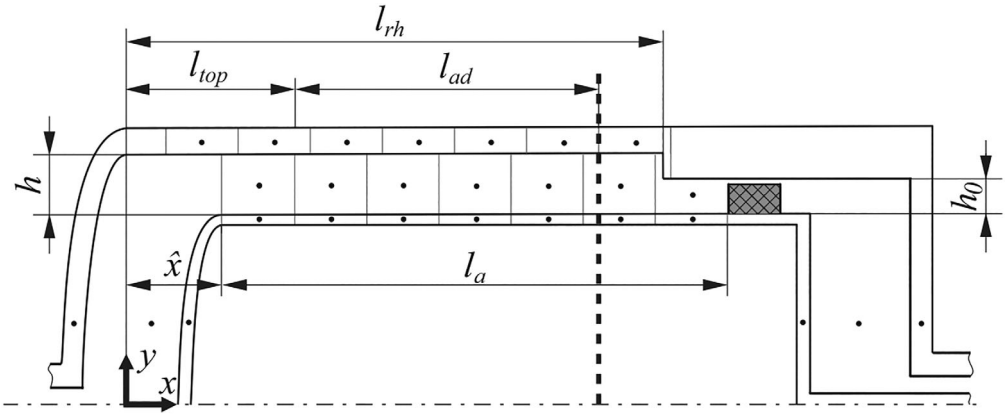

FIGURE 2 Discretization of the cylinder system including the appendix gap

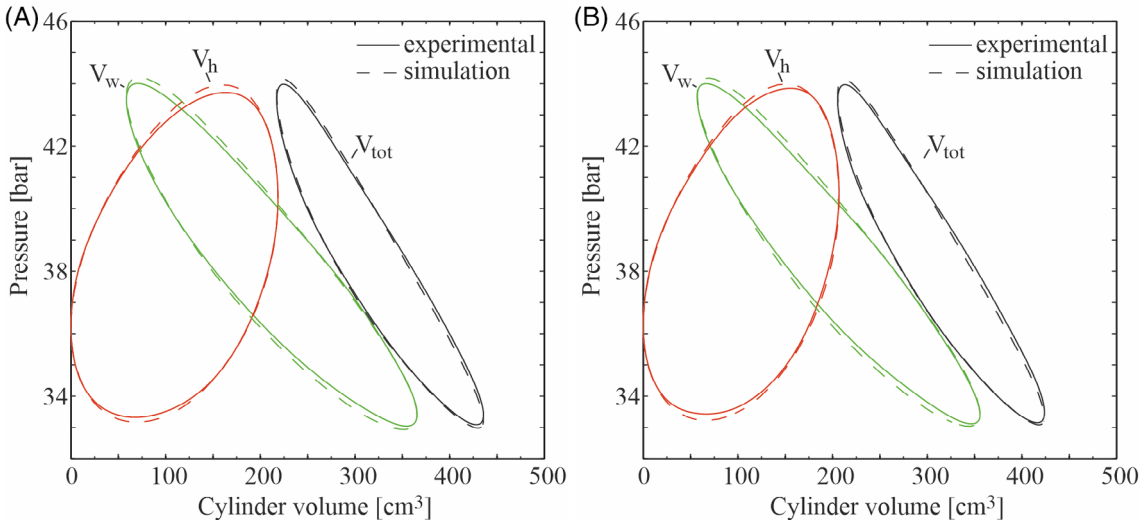

FIGURE 3 Simulated and measured p,V loops in Stirling mode with old[52] (A) and new (B) seal design

TABLE 1 Nominal operating conditions and geometric dimensions of the experimental machine

Parameter	Value	Parameter	Value
Heater temperature T_h	500°C	Cylinder internal bore	80 mm
Intermediate temperature T_w	30°C	Displacer stroke amplitude	21.75 mm
Working fluid	Helium	Gap width h	1.4 mm
Rotational speed n	383 minutes^{-1}	Bottom gap width h_0	0.3 mm
Mean pressure $\bar{p}$	38.3 bar	Gap width ratio (new seal design) r_h	0.21

refrigeration power. So, the agreement between the simulations and the experiments is generally satisfactory, allowing a closer look at the simulated appendix gap losses. For these, a large decrease is indicated by the simulation, confirming that a reduction of the diameter of the cylinder liner at the seal may significantly reduce the appendix gap loss.

Figure 5 shows the same comparison for Stirling mode operation. In this case, the simulation also confirms the experimental results concerning a reduced heat input, but once again, the reduction is lower for the simulated values. However, it is striking that despite the reduced displacement by the hot displacer, the simulated indicated power is also raised by the modified design, underlining the positive effect of the seal modification on the entire cycle and once again confirming the experimental results.

Additionally, it appears that in Stirling mode, the appendix gap loss is reduced by approximately the same amount as in Vuilleumier mode. However, the reduction of the heat input in Vuilleumier mode as well as in Stirling mode is larger than this, presumably due to the

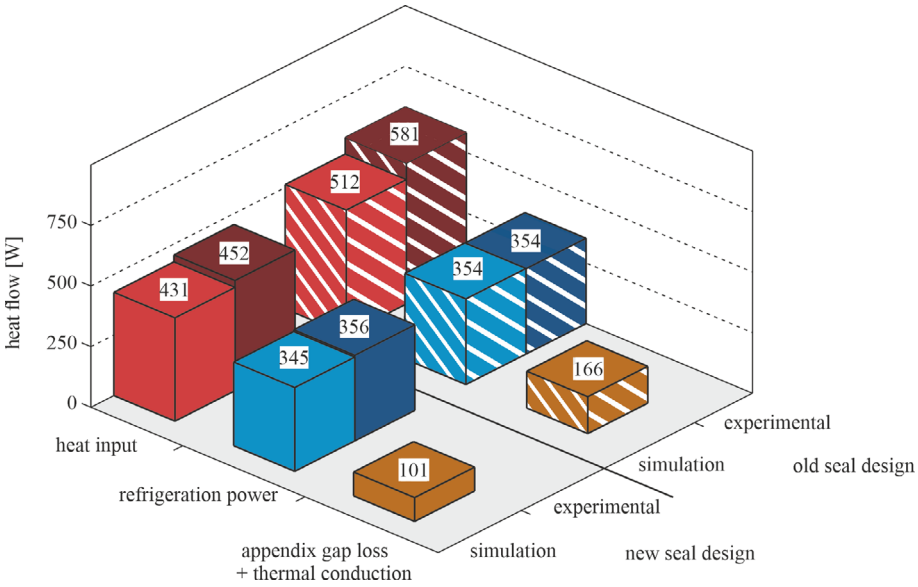

FIGURE 4 Simulated and measured heat input and refrigeration power in Vuilleumier mode for both seal designs

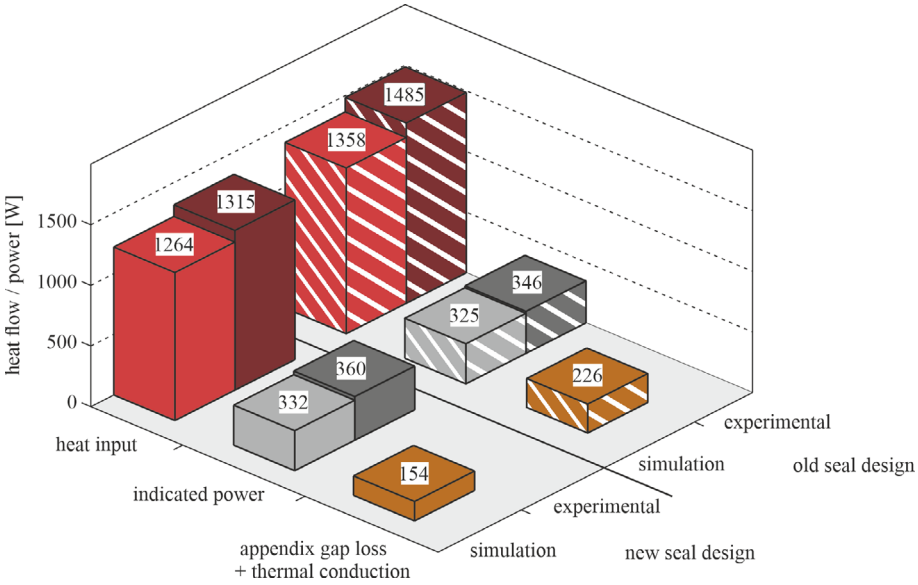

FIGURE 5 Simulated and measured heat input and indicated power in Stirling mode for both seal designs

aforementioned further positive effects, such as reduced thermal regenerator losses due to a decreased mass flow.

Furthermore, it should be considered that the appendix gap loss is an internal loss, i. e. any compensating heat flow imposes an additional load on both the heater and the cooler. A slightly increased heater gas temperature (+2 K) was observed in the simulation with the new seal design, thus confirming the anticipated positive effect on the pressure amplitude.[52]

2.2 | Numerical optimization of the seal design

Finally, the validated simulation model is applied to determine the optimum seal geometry, i. e. the optimum values for the width h and the gap width ratio r_h. In Figure 6, the simulated efficiency (a), i. e. the ratio of indicated power to heat input, and the simulated appendix gap loss plus heat conduction in Stirling mode (b) are plotted on the z-axis as a function of the gap width and the gap width ratio. The simulated values were additionally colored for better readability by mapping the minimum and maximum results on a color scale from red to blue. Values between simulations were linearly interpolated. Please note that the z-axis of the latter figure was reversed for reasons of better comparability.

The old seal design, which was obtained by minimization of the losses according to the analytical models by Rios[19] and Berchowitz,[28] and the new seal design are indicated by a black and a red arrow, respectively. In contrast to the previous results, these variations were performed under the constraint of a constant volumetric

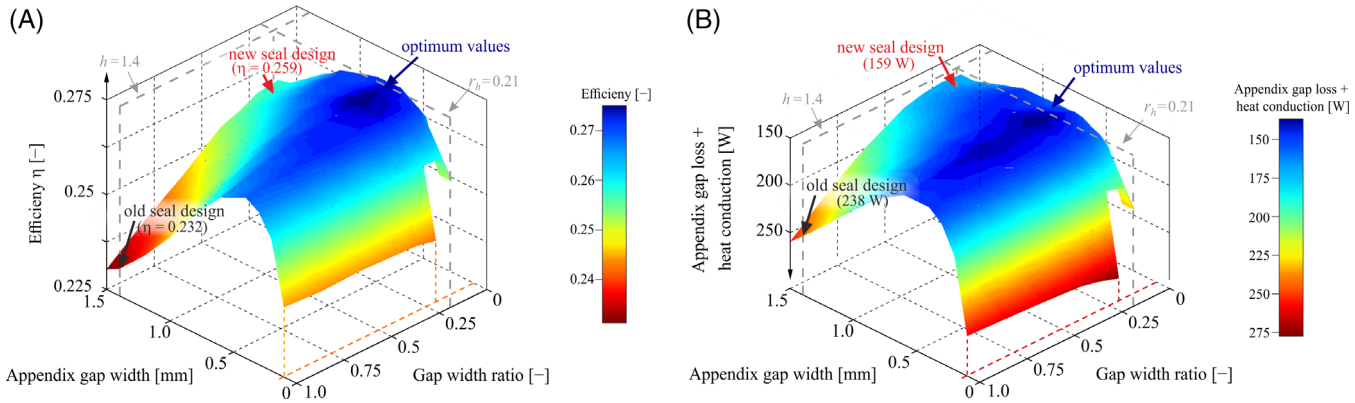

FIGURE 6 Simulated efficiency η (A) and appendix gap loss plus heat conduction (B) as a function of the appendix gap width and the gap width ratio in Stirling mode (old and new seal design indicated by black and red arrows, respectively)

displacement rather than a constant cylinder bore above the liner.

A comparison of both figures reveals that maximum efficiency almost coincides with the minimum appendix gap loss. Although the shapes of both planes are not completely identical, it is sufficient to consider only the efficiency in the following. Figure 6A clearly demonstrates that the design of the gap section has a very high impact on machine efficiency. However, the optimum is rather flat, particularly regarding r_h, and the optimum gap width is almost independent of the latter. Additionally, it is striking that the gap width of the old seal design (black arrow) is far away from the optimum, indicating that the analytical models by Rios[19] and Berchowitz[28] are not sufficiently detailed to predict the appendix gap loss satisfactorily.

In Vuilleumier mode, the machine parameter of interest to be optimized is the coefficient of performance (COP), i. e. the ratio of refrigeration power to heat input. The COP as a function of the gap width and the gap width ratio in Vuilleumier mode is visualized in Figure 7, again with both seal designs indicated by arrows.

It is obvious that the COP is largely affected by the gap design as well. However, the optimum width in Vuilleumier mode is far larger than in Stirling mode, whereas the optimum values for r_h are similar. Besides, it is interesting to compare the predicted optimum gap widths at a fixed r_h. In Stirling mode, the optimum gap width is always close to $h = 0.6$ mm for a given r_h, i. e. it is almost independent of r_h. In contrast, a strong dependency on r_h is found in Vuilleumier mode. In particular, the optimum gap width increases at smaller values for r_h. Conversely, the optimum values of r_h are always in the same range for any given gap width, i. e. the former is largely independent of the latter.

Lastly, the extensively tested GPU-3 Stirling engine shall serve as a reference case, since detailed experimental results and constructional information for this machine are available.[21,53-56] Sauer and Kühl[51] reported the corresponding simulation setup for the program *kpsim* and obtained a good agreement between experimental and simulated results. Figure 8 visualizes the efficiency of this engine as a function of the gap width and the gap width ratio. The real gap design is marked by a red arrow. Remarkably, the simulated optimum design of the gap is very close to the real design. Since no model for the appendix gap loss had been published at the time when the GPU-3 engine was developed, the gap and seal design was presumably optimized experimentally. Therefore, this good agreement may corroborate the accuracy of the simulation. Compared to the experimental machine, the optimum value for r_h is larger, underlining that its value - as well as the optimum gap width - is substantially dependent on the particular machine design. Just alike the experimental machine in Stirling mode, the optimum gap width appears to be almost independent of r_h.

3 | ANALYTICAL DETERMINATION OF THE OPTIMUM GAP GEOMETRY

3.1 | Phasor description of the spatial mean flow velocity

Obviously, the simulation provides a very useful tool for the optimization of the gap in regenerative cycles and illustrates the dependency of the optimum gap geometry on the specific machine design. However, demand for analytical calculation rules exists due to insufficient availability of such one-dimensional simulation tools, but so far, the analytical model by Pfeiffer and Kühl[44] provides a solution for the optimum gap width only. Sauer

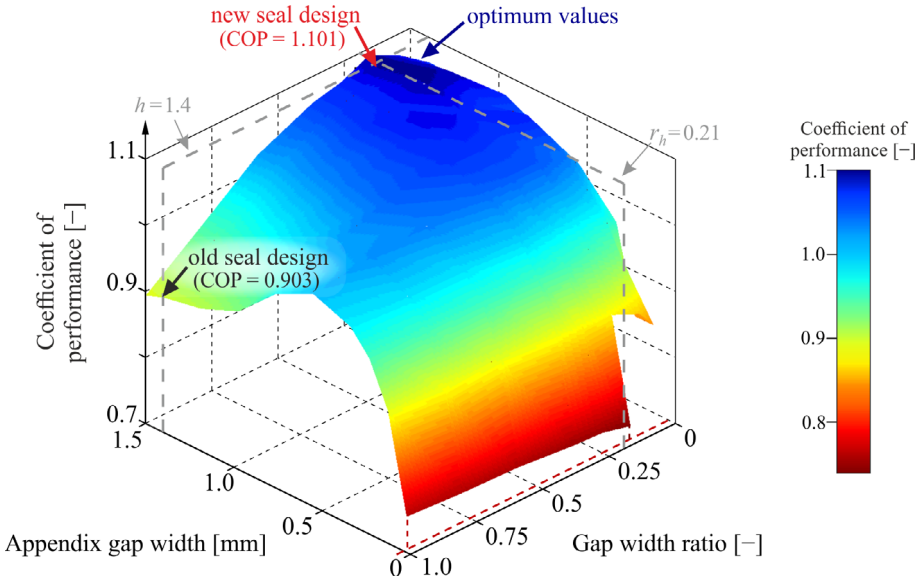

FIGURE 7 Simulated COP as a function of the appendix gap width and the gap width ratio in Vuilleumier mode (old and new seal design indicated by black and red arrow)

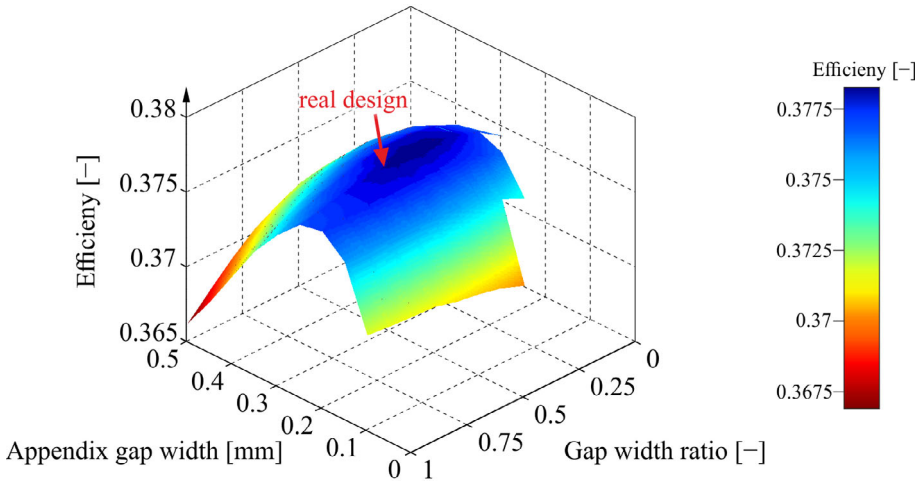

FIGURE 8 Simulated efficiency as a function of the appendix gap width and the gap width ratio in the GPU-3 engine (seal design indicated by red arrow)

and Kühl[49] were able to demonstrate that an optimized seal geometry particularly reduces the enthalpy loss due to reduced mass flows and flow velocities in the gap. Hence, these will be analyzed analytically in the following.

Based on the assumption of an ideal gas, the mass flow at the top of the gap may generally be derived by a linearized mass balance

$$\dot{m} = -\frac{\mathrm{d}m}{\mathrm{d}t} = \frac{-\overline{m}}{\overline{p}}\frac{\mathrm{d}p}{\mathrm{d}t} + \frac{-\overline{m}}{\overline{V_a}}\frac{\mathrm{d}V_a}{\mathrm{d}t} + \frac{\overline{m}}{\overline{T_m}}\frac{\mathrm{d}T_m}{\mathrm{d}t}. \qquad (2)$$

In this equation, p, m, V_a and T_m denote the pressure, the mass, the volume and the spatial mean temperature of the gas in the gap, and horizontal bars indicate temporal mean values. The individual components of the mass flow on the right-hand side of the equation may be illustrated vividly by a phasor description in the complex plane, based on the general assumption of sinusoidal motions and pressure fluctuations. In the following, this phasor system will be specified and illustrated.

Figure 9A presents the phasors for the displacer and the piston motion, x_D and x_P, for a γ-type Stirling engine (in black). Designating the cross-sectional areas of the displacer and its rod by A_D and A_R, respectively, the phasor of the hot volume amplitude is obtained as $\vec{V}_h = -A_D \cdot \overrightarrow{x_D}$. So, V_h is decreased by a positive displacement x_D, whilst the warm volume is contrarily increased since we have $\vec{V}_w = (A_D - A_R) \cdot \overrightarrow{x_D}$. Just alike, the piston volume is reduced by a positive displacement x_P, since the corresponding phasor is $\vec{V}_P = -A_P \cdot \overrightarrow{x_P}$, with the cross-sectional area of the piston A_P (green phasors). By the convention of Pfeiffer and Kühl,[43] the displacer velocity, which is the first derivative of the displacer position with respect to time $(dx_D/dt = \hat{x}\omega \cdot e^{i\omega t})$, is defined to have a zero phase angle. Generally, the first derivative of

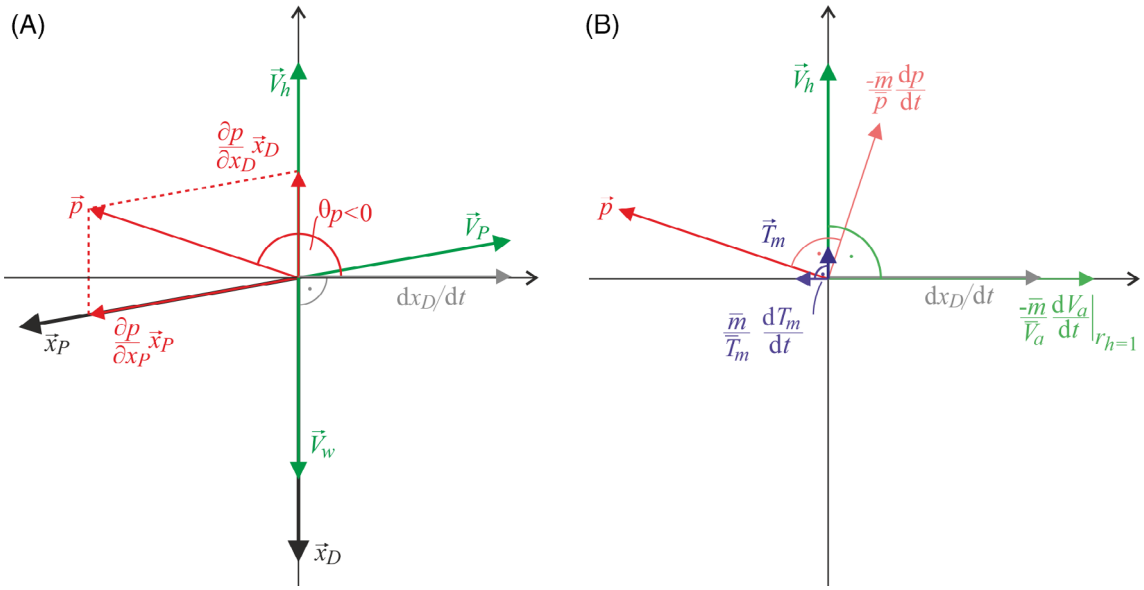

FIGURE 9 A, Phase relationships of volumes and pressure and B, phase relationships of derivatives

a phasor leads the original phasor by 90°, thus, by definition, x_D lags the zero phase by 90°. In phasor notation, the pressure phasor $\vec{p}$ may be obtained by superposition of the thermal and mechanical compression effects of the displacer and the piston:

$$\vec{p} = \frac{\partial p}{\partial x_p}\vec{x}_p + \frac{\partial p}{\partial x_D}\vec{x}_D. \tag{3}$$

The partial derivative $\partial p/\partial x_p$ quantifies the pressure change caused by a differential deflection of the piston while the displacer is considered to be at standstill in its mean position. Accordingly, the pressure change caused by the displacer is expressed by $\partial p/\partial x_D$. The pressure is defined as $p = \overline{p} + \hat{p} \cdot e^{i(\omega t - \Theta)}$. Thus, the pressure phasor lags the displacer velocity by the pressure phase angle θ_p. In the case shown in Figure 9A, where the pressure leads the displacer velocity, θ_p is therefore negative. Based on these specifications, the phasor $\frac{-\overline{m}}{\overline{p}}\frac{dp}{dt}$ lags the pressure by 90°, as indicated in Figure 9B. Since Equation (2) presents the mass flow across a boundary fixed to the cylinder wall, the volume in the gap V_a is decreased by a positive displacement x_D and thus, it is in phase with the hot volume. Thus, $\frac{-\overline{m}}{\overline{V}_a}\frac{dV_a}{dt}$ is graphically represented by a phasor lagging the hot volume by 90° as illustrated, i. e. its phase angle is zero. Obviously, the phase angle of this phasor is unaffected by the gap width ratio. In turn, the length of this phasor approaches zero for $r_h \to 0$. First of all, we examine the case for the maximum possible volumetric displacement at $r_h = 1$, denoted by $\frac{dV_a}{dt}\Big|_{r_h=1}$. Finally, it is assumed that the gas temperature at a fixed axial position in the gap is equal to the average of the adjacent wall temperatures. Hence, the average gas temperature T_m is decreased for a positive displacer deflection x_D, since the hot end of the displacer leaves the considered gap volume. However, the magnitude of this effect is decreased for $r_h \to 1$ due to the reduction of V_a at its cold end. Thus, the variation of T_m is in phase with the hot volume, and the phasor $\frac{\overline{m}}{\overline{T}_m}\frac{dT_m}{dt}$ leads the hot volume by 90° according to Figure 9B.

Vectorial addition of these three phasors yields the mass flow at the top of the gap as illustrated in Figure 10A. Now, assuming a temporally constant density ρ at the top of the gap, the spatial average flow velocity u_m is

$$u_m = \frac{\dot{m}}{\pi \cdot d_C \cdot h \cdot \rho}, \tag{4}$$

where d_C denotes the diameter of the cylinder bore. In dimensionless complex notation, the flow velocity is expressed as

$$\frac{\boldsymbol{u}_m}{\hat{x}\omega} = \Gamma \cdot e^{i(\omega t - \theta_u)} \text{ with } \Gamma = \frac{\hat{u}_m}{\hat{x}\omega}, \tag{5}$$

in accordance with the nomenclature by Pfeiffer and Kühl[43]. In this equation, Γ and θ_u denote the dimensionless flow velocity amplitude and the phase angle of the flow velocity relative to the displacer motion. Evidently, the spatial mean flow velocity is in phase with the mass flow, as also depicted in Figure 10A. Finally, the flow velocity in the system fixed to the cylinder wall may be

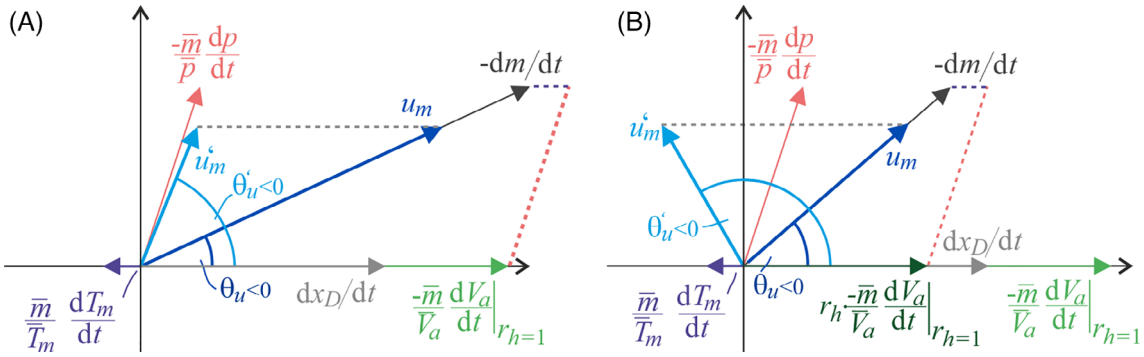

FIGURE 10 Phase relationships of mass flow and velocity at the top of the appendix gap A, normal seal design and B, reduced gap width ratio

transformed into the spatial mean flow velocity $\boldsymbol{u}'_m$ in the system moving with the displacer wall by.

$$\Gamma' \cdot e^{-i\theta'_u} = \Gamma \cdot e^{-i\theta u} - 1. \tag{6}$$

Here, $\Gamma' = \boldsymbol{u}'_m/\hat{x}\omega$ and θ'_u denote the dimensionless flow velocity amplitude and the phase angle of the flow velocity in the moving system. The corresponding phasor for $\boldsymbol{u}'_m$, as obtained by subtraction of dx_D/dt from u_m, is also shown in Figure 10A. If the volumetric displacement by the seal is reduced by $r_h < 1$, the second addend in Equation (2) expands to $r_h \cdot \frac{-\bar{m}}{\bar{V}_a}\frac{dV_a}{dt}\Big|_{r_h=1}$. The resulting new flow velocity is shown in Figure 10B for an arbitrarily chosen, $r_h = 0.5$. Obviously, r_h affects the amplitude as well as the phase angle of the flow velocity at the top of the gap, which is consistent with the presumptions derived from the experimental gas temperature results shown by Sauer and Kühl.[12]

However, this phasor description does not reveal the optimum gap width ratio or seal geometry. Therefore, Figure 11 shows the numerically simulated velocity (blue) and pressure phasors (red) at the optimum geometry (solid lines) as well as for $r_h = 1$ (dashed lines) in the experimental machine (a) Vuilleumier mode, (b) Stirling mode and (c) the GPU-3 Stirling engine. Please note the different scales of the figures, as indicated by the magnitude of the displacer velocity phasor, dx_D/dt.

Evidently, the flow velocity in the moving system in Vuilleumier mode is very small in contrast to those in Stirling mode and in the GPU-3 at the respective optimum design points. This induces a very small enthalpy loss and may explain the dependency of the optimum gap width on r_h. In simple terms, the shuttle loss features a reciprocal dependency, whereas, for the enthalpy loss, this dependency is linear, yielding an optimum gap width as a compromise between both loss mechanisms. However, by largely decreasing the flow velocity, the enthalpy loss almost vanishes, and the gap width may be enlarged considerably to reduce the shuttle loss. Contrarily, for considerably large velocity amplitudes, i. e. for non-ideal gap width ratios in Vuilleumier mode or generally in Stirling mode, the gap width cannot be increased to a large extent without substantially raising the enthalpy loss, and thus, medium values are obtained for the optimum gap widths in these cases. Apparently, it is not possible to reduce the flow velocity in Stirling mode to the same extent. This may be mainly attributed to the substantial mechanical compression by the piston inducing a velocity component perpendicular to the displacer velocity in case of a 90° shift between displacer and piston motion. Obviously, this component is unaffected by the choice of r_h. Consequently, simulated flow velocities in the moving system in Figure 11B,C are approximately 90° phase-shifted to the displacer velocity at the optimum design, whereas in Vuilleumier mode, the result is slightly different due to generally negligible flow velocities. As a rule of thumb, optimization of the gap width ratio r_h may therefore be reduced to a minimization of the flow velocity component that is in phase with the displacer motion. For this purpose, the velocity at the top of the gap must be evaluated analytically. This was done by Pfeiffer and Kühl,[44] who considered the influence of temporal temperature fluctuations to be negligible. However, Figure 10 illustrates that the influence of temperature fluctuations and the volumetric displacement by the seal feature diametrical effects canceling out to some extent. Thus, neglection of temperature fluctuations would yield too small gap width ratios, and temperature fluctuations should therefore be considered.

3.2 | Analytical determination of the flow velocity in the appendix gap

The determination of the flow velocities is based on a refinement of the mass balance in Equation (2) by three different sections featuring different temperature

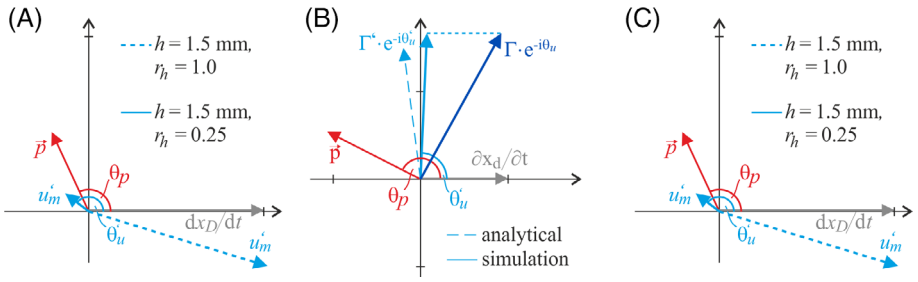

FIGURE 11 Simulated flow velocity at the top of the gap (moving system) for the optimum seal design compared to $r_h = 1$: A, Vuilleumier mode; B, Stirling mode; and C, GPU-3 Stirling engine

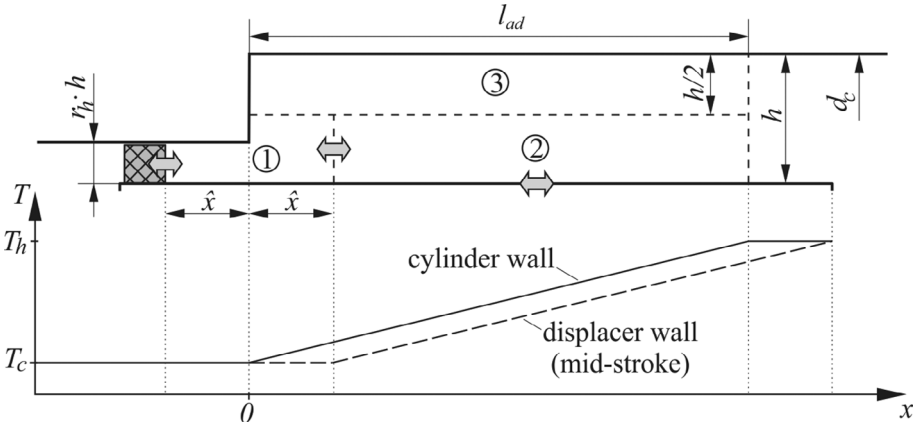

FIGURE 12 Sections and dimensions in the gap for derivation of flow velocity with the displacer at the mid-stroke position

distributions and partially undergoing volumetric changes. This segmentation is based on the idea that the gas locally has the average temperature of the surrounding walls and therefore, the gas may be notionally split into one half that is at the cylinder wall temperature and one half that is at the displacer wall temperature. Figure 12 shows these sections and the temperature profiles in the walls for the displacer mid-stroke position.

It is assumed that the gas in Sections (2) and (3) has the local displacer wall temperature $T_D(x)$ or the local cylinder wall temperature $T_{Cw}(x)$, respectively. Furthermore, constant temperature gradients in the displacer and the cylinder wall with an axial offset $\hat{x}$ at mid-stroke position are assumed, as indicated in Figure 12. Such an offset was observed in the numerical simulation particularly for small gap widths, when the isothermal bottom section (right-hand side), which is maintained at the cold temperature T_c, imposes its temperature on the facing displacer wall near the bottom dead center position of the displacer (ie, when the displacer is near the right end of stroke in this illustration). In contrast, the upper end of the cylinder is assumed to be at the hot temperature T_h. The gas in Section (1) is therefore assumed to be isothermal at T_c, and the length of this section is $2 \cdot \hat{x}$ and therefore constant. Its lower boundary is bound to the seal, and thus its volume $V_{bot}(x)$ undergoes volumetric changes for $r_h \neq 0.5$. Section (2) also undergoes volumetric changes, as its lower end is defined by the upper end of Section (1) and its upper boundary is fixed to the cylinder wall. Additionally, the gas in this section undergoes fluctuations of its spatial mean temperature. Finally, Section (3) is entirely bound to the cylinder wall and does not undergo any volumetric changes or fluctuations of the spatial mean temperature. The total mass in the gap below an arbitrarily chosen position $x \geq \hat{x}$ is therefore

$$m(x,t) = \frac{p(t) \cdot V_{bot}(t)}{R \cdot T_c} + \frac{p(t) \cdot V_D(x,t)}{R \cdot T_{D,m}(x,t)} + \frac{p(t) \cdot V_{Cw}(x)}{R \cdot T_{Cw,m}(x)}, \quad (7)$$

where V_D, V_{Cw}, $T_{D,m}$ and $T_{Cw,m}$ denote the volumes and the spatial mean temperatures of Sections (2) and (3), respectively, and R designates the specific gas constant. Based on this, and by linearization around mid-stroke position, the mass flow at the top is

$$\dot{m} = -\frac{\overline{p} \cdot V_a}{R \cdot T_c} \left\{ \left[\frac{\overline{V}_{bot}}{\overline{V}_a} + \frac{V_{Cw}}{\overline{V}_a} \frac{T_c}{T_{Cw,m}} + \frac{\overline{V}_D}{\overline{V}_a} \frac{T_c}{T_{D,m}} \right] \cdot \frac{1}{\overline{p}} \frac{\mathrm{d}p}{\mathrm{d}t} + \frac{1}{\overline{V}_a} \frac{\mathrm{d}V_{bot}}{\mathrm{d}t} + \frac{T_c}{\overline{V}_a} \cdot \frac{\mathrm{d}}{\mathrm{d}t} \left(\frac{V_D}{T_{D,m}} \right) \right\}, \quad (8)$$

with $\overline{V}_a = \pi \cdot d_c \cdot h \cdot l_{ad}$, where l_{ad} denotes the length of the adiabatic section in the cylinder wall, which is assumed to be thermally insulated to the surrounding. The derivation of the individual terms is generally based on complex quantities and the assumption of sinusoidal fluctuations with respect to time. For example, the pressure is described by the complex function

$$\boldsymbol{p} = \overline{p} \cdot \left(1 + r_p \cdot e^{\mathbf{i}\left(\omega t - \theta_p\right)}\right);\ r_p = \frac{\widehat{p}}{\overline{p}}. \tag{9}$$

Additionally, it is assumed that the axial variations of the wall temperatures are linear. However, the analytical derivation of the mass flow is yet lengthy and therefore further elaborated in the Appendix.

Finally, the mass flow at the dimensionless axial position $x^* = x/l_{ad}$ is obtained as

$$\dot{m}(x^*) = -\frac{\overline{p} \cdot \overline{V}_a \cdot \omega \cdot e^{\mathrm{i}\,\omega t}}{R \cdot T_c}\left\{J(x^*) \cdot \mathrm{i} \cdot r_p \cdot e^{-\mathrm{i}\theta_p} - r_x r_h + r_T\left(x^*\right)\right\}, \tag{10}$$

with $r_x = \widehat{x}/l_{ad}$ and

$$r_T(x^*) = \frac{1}{2} r_x \left(1 - \frac{1}{\left(T_h/T_c - 1\right).[x^* - r_x] + 1}\right). \tag{11}$$

The compressibility of the gas in the gap $J(x^*)$ is given as

$$J(x^*) = r_x\left[\frac{1}{2} + r_h\right] + \frac{1}{2}\frac{\ln\left(\left(T_h/T_c - 1\right)x^* + 1\right)}{T_h/T_c - 1} + \frac{1}{2}\frac{\ln\left(\left(T_h/T_c - 1\right)[x^* - r_x] + 1\right)}{\left(T_h/T_c - 1\right)}.. \tag{12}$$

Generalizing Equations (4) and (5) for an arbitrary dimensionless position x^*, assuming an ideal gas with a temporally constant local density

$$\rho(x^*) = \frac{\overline{p}}{R \cdot T_{Cw}(x^*)}, \tag{13}$$

as a minor simplification and solving for the mass flow yields

$$\dot{m}(x^*) = \frac{\overline{p} \cdot \overline{V}_a \cdot \omega}{R \cdot T_{Cw}(x^*)} \cdot r_x \cdot \Gamma(x^*) \cdot e^{\mathrm{i}(\omega t - \theta_u(x^*))}. \tag{14}$$

Equating Equations (10) and (14), the dimensionless flow velocity $\Gamma(x^*)$ at a given position x^* and its phase angle $\theta_u(x^*)$ relative to the displacer velocity are then found to be

$$\Gamma(x^*) = \frac{T_{Cw}(x^*)}{T_c}\sqrt{\left(r_h - \frac{r_T(x^*)}{r_x} - \frac{r_p}{r_x} \cdot \sin\left(\theta_p\right) \cdot J(x^*)\right)^2 + \left(\frac{r_p}{r_x} \cdot \cos\left(\theta_p\right) \cdot J(x^*)\right)^2}, \tag{15}$$

and

$$\cot(-\theta_u(x^*)) = \frac{r_h - \frac{r_T(x^*)}{r_x} - \frac{r_p}{r_x} \cdot \sin\left(\theta_p\right) \cdot J(x^*)}{\frac{r_p}{r_x} \cdot \cos\left(\theta_p\right) \cdot J(x^*)}. \tag{16}$$

Finally converting these functions into the moving system according to Equation (6) yields

$$\Gamma'(x^*) = \frac{T_{Cw}(x^*)}{T_c}\sqrt{\left(r_h - \frac{r_T(x^*)}{r_x} - \frac{r_p}{r_x} \cdot \sin\left(\theta_p\right) \cdot J(x^*) - \frac{T_c}{T_{Cw}(x^*)}\right)^2 + \left(\frac{r_p}{r_x} \cdot \cos\left(\theta_p\right) \cdot J(x^*)\right)^2}, \tag{17}$$

and

$$\cot\left(-\theta_u'(x^*)\right)=\frac{r_h-\frac{r_T(x^*)}{r_x}-\frac{r_p}{r_x}\cdot\sin\left(\theta_p\right)\cdot J(x^*)-\frac{T_c}{T_{Cw}(x^*)}}{\frac{r_p}{r_x}\cdot\cos\left(\theta_p\right)\cdot J(x^*)}. \tag{18}$$

3.3 | Calculation method for optimum design

According to the considerations in Chapter 4.1 above, the optimum gap width ratio is obtained, if in the moving system, the component of the flow velocity that is in phase with the displacer velocity, i. e. the expression in the denominator of Equation (18), is minimized at the top of the gap, i. e. by equating this expression to zero for $x^*=1$:

$$r_{h,\mathrm{opt}}-\frac{r_T(x^*=1)}{r_x}-\frac{r_p}{r_x}.\sin\left(\theta_p\right)\cdot J\left(x^*=1,r_{h,\mathrm{opt}}\right)-\frac{T_c}{T_h}=0. \tag{19}$$

Inserting Equations (11) and (12) and solving for $r_{h,\mathrm{opt}}$ yields the conditional equation for the optimum gap width ratio

$$r_{h,\mathrm{opt}}=\frac{\frac{1}{2}-\frac{1}{2}\frac{1}{\left(T_h/T_c-1\right)(1-r_x)+1}+\left(\frac{1}{2}+\frac{\ln\left(\left(T_h/T_c\right)\cdot\left(\left(T_h/T_c-1\right)(1-r_x)+1\right)\right)}{2\cdot r_x\cdot\left(T_h/T_c-1\right)}\right)\cdot r_p\cdot\sin\left(\theta_p\right)+\frac{T_c}{T_h}}{1-r_p\cdot\sin\left(\theta_p\right)}. \tag{20}$$

Interestingly, for a piston lagging the displacer by exactly 90°, the term $r_p\cdot\sin(\theta_p)$ reduces to the pressure influence of the displacer $\partial p/\partial x_D\cdot\vec{x}_D$. Since thermal compression by the displacer is almost the same in the Stirling and Vuilleumier mode of the experimental machine, this explains why the optimum value of r_h is also almost the same for both modes. Knowing r_h, which is apparently independent of the gap width, the optimum gap width may easily be calculated in the last step, applying the formulas by Pfeiffer and Kühl,[44] which are reported here for reasons of completeness. The optimum gap width is obtained by determination of the optimum Péclet number for the axial center of the gap according to

$$Pe_{\omega,\mathrm{opt}}=\frac{16}{\left[\begin{array}{l}\frac{51}{35}\left[1-4\Gamma(0.5)\cdot\cos(\theta_u(0.5))+4\Gamma(0.5)^2\right]+\\ \frac{12}{5}\left[2\Gamma(0.5)\cdot\sin\left(\theta_u(0.5)-\theta_p\right)+\sin\left(\theta_p\right)\right]f+f^2\cos^2\left(\theta_p\right)\end{array}\right]^{\frac{1}{2}}-f\cos\left(\theta_p\right)}, \tag{21}$$

with

$$f=r_p\frac{(T_h+T_c)\cdot l_{ad}}{2\cdot\widehat{x}\cdot(T_h-T_c)}\frac{R}{c_p}, \tag{22}$$

where c_p denotes the isobaric heat capacity. The relative flow velocity amplitude Γ and its phase angle θ_u should be evaluated for $x^*=0.5$ and $T_{Cw}(x^*=0.5)=(T_h+T_c)/2$ according to Equations (15) and (16), thus once again including the refined consideration of temperature effects in these equations as a further enhancement of the aforementioned model. Having determined the thermal diffusivity of the gas at this temperature, the optimum gap width is finally obtained as

$$h_{\mathrm{opt}}=\frac{1}{2}\sqrt{\frac{Pe_{\omega,\mathrm{opt}}\cdot a\left(\frac{T_h+T_c}{2}\right)}{\omega}}. \tag{23}$$

TABLE 2 Analytically calculated and simulated optimum gap design

	Experimental machine		
	Vuilleumier mode	**Stirling mode**	**GPU-3**
Simulation	$r_h = 0.25$; $h = 1.5$ mm	$r_h = 0.3$; $h = 0.6$ mm	$r_h = 0.55$; $h = 0.25$ mm
Analytical evaluation	$r_h = 0.36$; $h = 1.12$ mm	$r_h = 0.36$; $h = 0.67$ mm	$r_h = 0.7$; $h = 0.25$ mm
Simulation for $r_h = 1$	$h = 0.6$ mm	$h = 0.5$ mm	$h = 0.23$ mm
Analytical evaluation for $r_h = 1$	$h = 0.64$ mm	$h = 0.54$ mm	$h = 0.23$ mm

Thus, the gap geometry may be optimized on an analytical basis with regard to both r_h and the gap width for the first time. A comparison of the optimum values obtained by this method and by numerical simulation is given in Table 2. The optimum gap width values for a conventional design without a step, i. e. for $r_h = 1$, are also included.

Evidently, the analytical model yields gap designs very similar to the numerical optimization with the only exception of the Vuilleumier mode, where a slightly larger gap width ratio r_h is obtained analytically, which directly entails a smaller gap width. However, Figure 7 shows that the analytical solution is in the range of the plateau for efficiency and does not yield significantly higher losses. If in turn, the gap width ratio is fixed to $r_h = 1$, the results for the gap width are very similar again. Obviously, the new method is generally able to predict the optimum gap design at a good accuracy and may therefore be profitably applied in the design of regenerative machines.

4 | CONCLUSION

The experimentally proven decrease of losses in the appendix gap by a modified seal with a step in the cylinder wall was studied numerically and analytically for different modes of an experimental machine and for the well-known GPU-3 engine. The numerical reproduction required a modification of the simulation code, which proved to be sufficiently accurate. Using this code, the maximum deviations between experiments and simulations were up to 12% in the case of hot heat input and up to 3% and 8% in the case of refrigeration power and indicated power, respectively. However, it was possible to satisfactorily reproduce the experimentally observed effects and improvements in Vuilleumier mode as well as in Stirling mode. Subsequent optimizations revealed, that the optimum step size depends on the particular machine design and may in turn largely affect the optimum gap width, since the enthalpy loss may be minimized by an appropriate choice of the step width. As a consequence, the gap width may be increased, thus also reducing the shuttle loss. For the actual gap size of the experimental machine, the simulation predicts that the efficiency in Stirling mode can be increased from 23.2% to 25.9%.

The phasor analysis performed in this contribution revealed that it is essential to consider the amplitude and phase angle of the cycle pressure as well as the operating temperatures to determine the optimum gap width ratio correctly. This was finally achieved by minimization of the flow velocity relative to the displacer velocity at the top of the gap applying an extended, though of course partially simplified and linearized analytical model for this flow velocity including temperature fluctuations, pressure fluctuations and the volumetric displacement by the seal. Subsequently, the optimum gap width may be evaluated based on an existing analytical model, although using the refined model for the flow velocities. Thus, a rather simple, fully analytical optimization method for the major parameters yielding a minimized appendix gap loss could be derived. Despite its inevitable simplifications, the predicted optimum gap design is found to be in good accordance with numerical results and to be sufficiently accurate under practical aspects. Furthermore, the model contributes to a better theoretical understanding of the essential mechanisms generating the appendix gap loss.

ACKNOWLEDGEMENT

This research was funded by the German Research Foundation (DFG), grant number KU 755/4-1 & 2. Open access funding enabled and organized by Projekt DEAL.

CONFLICT OF INTEREST

The authors declare no conflict of interest. The funders had no role in the design of the study; in the collection, analyses, or interpretation of data; in the writing of the manuscript, or in the decision to publish the results.

NOMENCLATURE

A	area, m^2
a	thermal diffusivity, m^2/s
c_p	isobaric heat capacity, J/kgK
d	diameter, m

f	constant (Equation [22])
h	appendix gap width, m
$\boldsymbol{i}$	imaginary unit
J	compressibility factor
l	length, m
m	mass, kg
Pe_ω	kinetic Péclet number ($Pe_\omega = 4h^2\omega/a$)
p	pressure, bar
R	specific gas constant, J/kgK
r_h	gap width ratio
r_p	dimensionless pressure amplitude
r_T	dimensionless temperature amplitude
r_x	dimensionless stroke amplitude
T	temperature,°C
t	time, s
u	velocity, m/s
V	volume, m^3
$\hat{x}$	stroke amplitude, m
x	axial coordinate, m

GREEK LETTERS

Γ	dimensionless flow velocity amplitude
θ_p	pressure phase angle relative to displacer velocity
θ_u	velocity phase angle relative to displacer velocity
λ	thermal conductivity, W/mK
ν	kinematic viscosity
ρ	density, kg/m^3
ω	angular velocity, min^{-1}

SUBSCRIPTS

a	appendix gap
ad	adiabatic
bot	bottom end of the cylinder wall
C	cylinder
c	cold
D	displacer
h	hot
m	spatial mean
opt	optimum
P	piston
R	rod

SUPERSCRIPTS

$\bar{}$	temporal average
$\hat{}$	amplitude
$'$	relative system bound to the displacer
$\cdot$	time derivative

DATA AVAILABILITY STATEMENT

Data sharing is not applicable to this article as no new data were created or analyzed in this study.

ORCID

Hans-Detlev Kühl https://orcid.org/0000-0001-8110-1134

REFERENCES

1. Aranceta J, Lopez A, del Portal XR. The long road from laboratory to market with stirling microgeneration systems. Paper presented at: Proceedings International Stirling Forum (ed ZUK der DBU). International Stirling Forum, September 23-24, 2008, Osnabrück, 2008.
2. Alanne K, Paatero J, Beausoleil-Morrison I. Performance assessment of a Stirling engine plant for local micro-cogeneration. *Int J Energy Res*. 2012;36(2):218-230.
3. Rogdakis ED, Antonakos GD, Koronaki IP. Thermodynamic analysis and experimental investigation of a solo V161 Stirling cogeneration unit. *Energy*. 2012;45:503-511.
4. Grosu L, Dobre C, Petrescu S. Study of a Stirling engine used for domestic micro-cogeneration. Thermodynamic analysis and experiment. *Int J Energy Res*. 2015;39(9):1280-1294.
5. Thomas B, Wyndorps A, Böhnisch H, Lemmer A, Oechsner H, Vogtherr J. Field testing of small Stirling CHP's running on bio-, mine and sewage gas. Paper presented at: Proceedings International Stirling Forum (ed ZUK der DBU). International Stirling Forum, Osnabrück, 2006, p. 10.
6. Silva Lora EE, Mahkamov K, Martinez JD, Andrade RV, Cobas V. A 50-kWth two-stage downdraft biomass gasifier for application with internal and external conbustion engines. Paper presented at: Proceedings 14th ISEC (ed International Stirling Association). 14th ISEC, Groningen, 2009.
7. Obara S, Kito S, Hoshi A, Sasaki S. Study on woody biomass Stirling cycle for cold region houses. *Int J Energy Res*. 2009;33(2):152-163.
8. Harrod J, Mago PJ, Luck R. Sizing analysis of a combined cooling, heating, and power system for a small office building using a wood waste biomass-fired Stirling engine. *Int J Energy Res*. 2012;36(1):64-74.
9. Brandt H-J, Frauscher J, Höftberger E, Aigenbauer S, Mair C. Stir-Bio: Demonstration of the Performance of a Stirling Engine Fired by Wood Pellet Combustion. Paper presented at: Proceedings 18th ISEC (ed International Stirling Association). 18th ISEC, Tainan, Taiwan, 2018, pp. 114–121.
10. Marra FS, Miccio F, Solimene R, Chirone R, Urciuolo M, Miccio M. Coupling a Stirling engine with a fluidized bed combustor for biomass. *Int J Energy Res*. 2020;44(15):12572–12582.
11. Acampora L, Continillo G, Marra F, Miccio F, Urciuolo M. Development of an experimental test rig for cogeneration based on a Stirling engine and a biofuel burner. *Int J Energy Res*. 2020;44(15):12559–12571.
12. Mahkamov K, Eid EI. Technical feasibility study of a concept of a medium temperature Stirling engine solar power unit. Paper presented at: Proceedings 14th ISEC (ed International Stirling Association). 14th ISEC, Groningen, 2009.
13. Renzi M, Bartolini CM, Santolini M. Investigation on the thermal performance of an innovative receiver for a solar dish system. Paper presented at: Proceedings 15th ISEC (ed International Stirling Association). 15th ISEC, Dubrovnik, 2012.

14. Oriti SM. Performance measurement of advanced stirling convertors (ASC-E3). Paper presented at: Proceedings 11th IECEC (ed American Institute of Aeronautics and Astronautics). 11th IECEC, San Jose, California. American Institute of Aeronautics and Astronautics Inc., Reston, Virginia, 2013.
15. Daoud JM, Friedrich D. A new duplex Stirling engine concept for solar-powered cooling. *Int J Energy Res*. 2020;44(7):6002-6014.
16. Walker G, Senft JR. *Free Piston Stirling Engines*. Berlin: Springer-Verlag; 1985.
17. Zare S, Tavakolpour-Saleh A. Free piston Stirling engines: a review. *Int J Energy Res*. 2020;44(7):5039-5070.
18. Zimmerman FJ, Longsworth RC. Shuttle Heat Transfer. Paper presented at: Cryogenic Engineering Conference, 5th edn. Cryogenic Engineering Conference, Boulder, Colorado. Plenum Press, New York, 1971, pp. 342–351.
19. Rios PA. An approximate solution to the shuttle heat-transfer losses in a reciprocating machine. *J Eng Gas Turbines Power*. 1971;93:177-182.
20. Harness JB, Newmann PEL. A Theoretical Solution of Shuttle Heat Transfer Problem. Paper presented at: 4th International Cryogenic Conference. 4th International Cryogenic Conference, Eindhoven; 1972, pp. 97–100.
21. Urieli I, Berchowitz DM. *Stirling Cycle Engine Analysis*. Bristol: Adam Hilger Ltd; 1984.
22. Huang SC. Appendix Gap Loss in Stirling Engines, Analysis and User's Manual: NASA Contract DEN3-32, Mechanical Technology Incorporated (MTI), Latham, NY; 1985.
23. Radebaugh R, Zimmerman JE. Shuttle Heat Transfer in Plastic Displacers at Low Speeds: NBS Special Publications.
24. Berchowitz DM. Stirling Cycle Engine Design and Optimization: Faculty of Engineering. University of the Witwatersrand, Johannesburg. Dissertation; 1986.
25. Huang SC, Berggren RW. Evaluation of Stirling Engine Appendix Gap Losses. Paper presented at: Proc. 21st IECEC, 869133rd edn (ed American Institute of Aeronautics and Astronautics). 21st IECEC, San Diego, CA, 1986, pp. 562–568.
26. McMahon HO, Gifford WE. A new low-temperature gas expansion cycle-part I. *Adv Cryog Eng*. 1960;5:354-367.
27. Walker G. *Cryocoolers; Part 2: Applications*. New York and London: Plenum Press; 1983.
28. Berchowitz DM, Berggren RW. Appendix Gap Losses in Reciprocating Machines.
29. Ibrahim MB, Mittal M, Simon TW, Gedeon D. A 2- D CFD Model of a Free Piston Stirling Engine for Space Applications with Annular Heat Exchangers. Paper presented at: Proceedings 2nd IECEC, 2004th edn (ed American Institute of Aeronautics and Astronautics). Proc. 2nd IECEC, Providence, Rhode Island.American Institute of Aeronautics and Astronautics Inc., Reston, Virginia, 2004.
30. Wilson SD, Dyson RW, Tew RC, Jr, Ibrahim MB. Multi-D CFD Modeling of a Free-Piston Stirling Convertor at NASA Glenn. Paper presented at: Proceedings 2nd IECEC, 2004th edn (ed American Institute of Aeronautics and Astronautics). Proc. 2nd IECEC, Providence, Rhode Island.American Institute of Aeronautics and Astronautics Inc., Reston, Virginia, 2004.
31. Mahkamov K. An axisymmetric computational fluid dynamics approach to the analysis of the working process of a solar Stirling engine. *J Sol Energy Eng*. 2006;128:45-53.
32. Chen W-L, Yang Y-C, Salazar JL. A CFD parametric study on the performance of a low-temperature-differential γ-type Stirling engine. *Energy Convers Manag*. 2015;106:635-643.
33. Chen W-L. A study on the effects of geometric parameters in a low-temperature-differential γ -type Stirling engine using CFD. *Int J Heat Mass Transfer*. 2017;107:1002-1013.
34. Xiao G, Sultan U, Ni M, et al. Design optimization with computational fluid dynamic analysis of ßtypeStirling engine. *Appl Therm Eng*. 2017;113:87-102.
35. Dogkas G, Rogdakis ED, Bitsikas P. 3D CFD simulation of a Vuilleumier heat pump. *Appl Therm Eng*. 2019;153:604-619.
36. Andersen SK. Numerical simulation of cyclic thermodynamic processes: Department of Mechanical Engineering. Technical University of Denmark Dissertation.
37. Andersen SK, Carlsen H, Thomsen PG. Preliminary results from a numerical study on the appendix gap losses in a Stirling engine. Paper presented at: Proceedings 12th ISEC (ed International Stirling Association). 12th ISEC, Durham UK, 2005, pp. 336–347.
38. Geue I, Pfeiffer J, Kühl H-D. Laboratory-scale Stirling-Vuilleumier hybrid system part II: experimental results. *J Propuls Power*. 2013;29:812-824.
39. Geue I, Pfeiffer J, Kühl H-D. Laboratory-scale Stirling-Vuilleumier hybrid system part I: application of similarity-based design. *J Propuls Power*. 2013;29:800-811.
40. Geue I. Entwicklung, ähnlichkeitstheoretischeSkalierung und Untersuchungeinesumschaltbaren Systems ausStirlingmotor und Vuilleumier-Wärmepumpezurdezentralen Hausenergieversorgung: Dissertation, LehrstuhlfürThermodynamik, TU Dortmund, SchriftenreiheThermodynamik, Dr. Hut, München; 2012.
41. Kühl H-D, Pfeiffer J, Sauer J. Operating Characteristics of a Laboratory-Scale, Convertible Stirling-Vuilleumier-Hybrid CHP System Including a Reversed-Rotation Stirling Mode. Paper presented at: Proceedings 16th ISEC (ed International Stirling Association). 16th ISEC, Bilbao, Spain, 2014, pp. 294–304.
42. Pfeiffer J, Kühl H-D. Review of models for appendix gap losses in Stirling cycle machines. *J Propuls Power*. 2014;30:1419-1432.
43. Pfeiffer J, Kühl H-D. New analytical model for appendix gap losses in Stirling cycle machines. *J Thermophys Heat Transf*. 2016;30:288-300.
44. Pfeiffer J, Kühl H-D. Optimization of the appendix gap Design in Stirling Engines. *J Thermophys Heat Transf*. 2016;30:831-842.
45. Pfeiffer J. Unsteady Analytical Model for Appendix Gap Losses in Stirling Cycle Machines: Dissertation, LehrstuhlfürThermodynamik, TU Dortmund, SchriftenreiheThermodynamik, Dr. Hut, München, 2016.
46. Karabulut H, Çınar C, Aksoy F. The investigation of the effect of thermal barrier coating on the performance of Stirling engine. *Int J Energy Res*. 2009;33(3):267-273.
47. Karabulut H, Çınar C, Aksoy F, Yücesu HS. Improved Stirling engine performance through displacer surface treatment. *Int J Energy Res*. 2010;34(3):275-283.
48. Baik JH, Chang HM. An exact solution for shuttle heat-transfer. *Cryogenics*. 1995;35:9-13.
49. Sauer J, Kühl H-D. Experimental investigation of displacer seal geometry effects in Stirling cycle machines. *Energies*. 2019;12(21):4215.

50. Sauer J, Kühl H-D. Analysis of unsteady gas temperature measurements in the appendix gap of a Stirling engine. *J Propuls Power*. 2018;34:1039-1051.
51. Sauer J, Kühl H-D. Numerical model for Stirling cycle machines including a differential simulation of the appendix gap. *Appl Therm Eng*. 2017;111:819-833.
52. Sauer J, Kühl H-D. Theoretically and experimentally founded simulation of the appendix gap in regenerative machines. *Appl Therm Eng*. 2020;166:114530.
53. Thieme LG, Tew RC, Jr. Baseline performance of the GPU-3 Stirling engine: NASA TM-79038, 1978.
54. Thieme LG. Low-Power Baseline Test Results for the GPU 3 Stirling Engine: NASA Technical Memorandum 79103, 1979.
55. General Motors Research Laboratories A collection of Stirling engine reports from General Motors' research, 1958 to 1970, Part 6: Fachinformationszentrum Energie Physik Mathematik GmbH.
56. Tew RC, Jr, Thieme LG, Miao D. Initial comparison of single cylinder Stirling engine computer model predictions with test results, in SAE Technical Paper Series, Tagung Z 1394 (790327). SAE Technical Paper Series, Tagung Z 1394 (790327), 1979.

How to cite this article: Sauer J, Kühl H-D. Performance improvements in Stirling cycle machines by a modified appendix gap geometry. *Int J Energy Res*. 2022;46(2):1180-1197. doi: 10.1002/er.7237

APPENDIX: ANALYTICAL DERIVATION OF THE MASS FLOWS IN THE GAP

Assuming a sinusoidal displacer motion and introducing $x^* = x/l_{ad}$ and $r_x = \hat{x}/l_{ad}$, the volumes of the three sections may be expressed as complex quantities:

$$V_{Cw}(x^*) = \frac{1}{2}\overline{V}_a \cdot x^*; \tag{A1}$$

$$V_D(x^*,t) = \frac{1}{2}\overline{V}_a\left[x^* - r_x\left(1 - \mathrm{i}\, e^{\mathrm{i}\omega t}\right)\right]; \tag{A2}$$

$$V_{bot}(t) = \overline{V}_a \cdot r_x\left[\frac{1}{2}\left(1 - \mathrm{i}\, e^{\mathrm{i}\,\omega t}\right) + r_h\left(1 + \mathrm{i}\, e^{\mathrm{i}\,\omega t}\right)\right]. \tag{A3}$$

Hence, the temporal mean values and the time derivatives are obtained as

$$\begin{aligned} \frac{\overline{V}_D(x^*)}{\overline{V}_a} &= \frac{1}{2}\left[x^* - r_x\right], \\ \frac{\overline{V}_{bot}}{\overline{V}_a} &= r_x\left[\frac{1}{2} + r_h\right], \end{aligned} \tag{A4}$$

$$\frac{1}{\overline{V}_a}\frac{\mathrm{d}V_D}{\mathrm{d}t} = -\omega \cdot \frac{r_x}{2} e^{\mathrm{i}\,\omega t} \text{ and } \frac{1}{\overline{V}_a}\frac{\mathrm{d}V_{bot}}{\mathrm{d}t} = \omega \cdot r_x\left[\frac{1}{2} - r_h\right] e^{\mathrm{i}\omega t}. \tag{A5}$$

The temperatures in the displacer and the cylinder wall are assumed to be linear functions of the axial position:

$$\begin{aligned} T_D(x^*,t) &= T_c + (T_h - T_c)\cdot\left(x^* - r_x\left(1 - \mathrm{i}\, e^{\mathrm{i}\,\omega t}\right)\right); \\ T_{Cw}(x^*) &= T_c + (T_h - T_c)\cdot x^*. \end{aligned} \tag{A6}$$

The spatial mean temperatures in the displacer wall and the cylinder wall should be evaluated as logarithmic mean temperatures, and hence, one obtains

$$\begin{aligned} T_{D,m}\left(x^*\right) &= \frac{\left|x^* - r_x\left(1 - \mathrm{i}\, e^{\mathrm{i}\,\omega t}\right)\right|(T_h - T_c)}{\ln\left(\left({}^{T_h}\!/_{T_c} - 1\right)\left[x^* - r_x\left(1 - \mathrm{i}\, e^{\mathrm{i}\,\omega t}\right)\right] + 1\right)} \text{ and} \\ T_{Cw,m}(x^*) &= \frac{x^*(T_h - T_c)}{\ln\left(\left({}^{T_h}\!/_{T_c} - 1\right)x^* + 1\right)}. \end{aligned} \tag{A7}$$

Now, we can write

$$\frac{\overline{V}_{Cw}}{\overline{V}_a}\frac{T_c}{T_{Cw,m}} = \frac{1}{2}J_1(x^*) \text{ and } \frac{\overline{V}_D}{\overline{V}_a}\frac{T_c}{T_{D,m}} = \frac{1}{2}J_2(x^*), \tag{A8}$$

with

$$\begin{aligned} J_1(x^*) &= \frac{\ln\left(\left({}^{T_h}\!/_{T_c} - 1\right)x^* + 1\right)}{{}^{T_h}\!/_{T_c} - 1} \text{ and} J_2(x^*) \\ &= \frac{\ln\left(\left({}^{T_h}\!/_{T_c} - 1\right)\left[x^* - r_x\right] + 1\right)}{\left({}^{T_h}\!/_{T_c} - 1\right)}. \end{aligned} \tag{A9}$$

Inserting all these expressions in Equation (8) finally yields

$$\begin{aligned} \dot{m} = &-\frac{\overline{p}\cdot\overline{V}_a\cdot\omega\cdot e^{\mathrm{i}\,\omega t}}{R\cdot T_c} \\ &\left\{\left[r_x\left(\frac{1}{2} + r_h\right) + \frac{1}{2}\left(J_1(x^*) + J_2(x^*)\right)\right]\cdot\right. \\ &\left.\mathrm{i}\cdot r_p\cdot e^{-\mathrm{i}\,\theta_p} - r_x\cdot r_h + \frac{r_x}{2} - \frac{r_x}{2}\frac{1}{\left({}^{T_h}\!/_{T_x} - 1\right)\cdot\left[x^* - r_x\right] + 1}\right\}. \end{aligned} \tag{A10}$$

From Equation (2), it is obvious that the mass flow is generally induced by three effects, namely by the pressure change, the change of the spatial mean temperature

and the volumetric change. Knowing that the former is the term including r_p and the latter includes $\frac{1}{\overline{V}_a}\frac{dV_a}{dt} = -\omega \cdot r_x \cdot r_h e^{\mathrm{i}\,\omega t}$, we can condense the influence of the temperature fluctuations to

$$r_T(x^*) = \frac{1}{2} r_x \left(1 - \frac{1}{\left(T_h/T_c - 1\right) \cdot [x^* - r_x] + 1}\right). \tag{A11}$$

Moreover, the compressibility of the gas can be abbreviated as $J(x^*) = r_x\left[\frac{1}{2} + r_h\right] + \frac{1}{2}J_1(x^*) + \frac{1}{2}J_2(x^*)$ and the mass flow is finally obtained as

$$\dot{m} = -\frac{\overline{p} \cdot \overline{V}_a \cdot \omega \cdot e^{\mathrm{i}\,\omega t}}{R \cdot T_c}\left\{J(x^*) \cdot \mathrm{i} \cdot r_p \cdot e^{-\mathrm{i}\,\theta_p} - r_x r_h + r_T(x^*)\right\}. \tag{A12}$$